JACS
JOURNAL OF THE AMERICAN CHEMICAL SOCIETY
COMMUNICATION
pubs.acs.org/JACS

Ligand Topology Effect on the Reactivity of a Mononuclear Nonheme Iron(IV)-Oxo Complex in Oxygenation Reactions

Seungwoo Hong,[†,‡,§] Yong-Min Lee,[†,§] Kyung-Bin Cho,[†] Karuppasamy Sundaravel,[†] Jaeheung Cho,[†] Myoung Jin Kim,[†] Woonsup Shin,[*,‡] and Wonwoo Nam[*,†]

[†]Department of Bioinspired Science, Ewha Womans University, Seoul 120-750, Korea

[‡]Department of Chemistry and Interdisciplinary Program of Integrated Biotechnology, Sogang University, Seoul 121-742, Korea

Supporting Information

ABSTRACT: Mononuclear nonheme iron(IV)-oxo complexes with two different topologies, *cis*-α-[$\mathrm{Fe^{IV}(O)(BQCN)}$]$^{2+}$ and *cis*-*β*-[$\mathrm{Fe^{IV}(O)(BQCN)}$]$^{2+}$, were synthesized and characterized with various spectroscopic methods. The effect of ligand topology on the reactivities of nonheme iron(IV)-oxo complexes was investigated in C−H bond activation and oxygen atom-transfer reactions; *cis*-α-[$\mathrm{Fe^{IV}(O)(BQCN)}$]$^{2+}$ was more reactive than *cis*-*β*-[$\mathrm{Fe^{IV}(O)(BQCN)}$]$^{2+}$ in the oxidation reactions. The reactivity difference between the *cis*-α and *cis*-*β* isomers of [$\mathrm{Fe^{IV}(O)(BQCN)}$]$^{2+}$ was rationalized with the $\mathrm{Fe^{IV/III}}$ redox potentials of the iron(IV)-oxo complexes: the $\mathrm{Fe^{IV/III}}$ redox potential of the *cis*-α isomer was 0.11 V higher than that of the *cis*-*β* isomer.

Since the first crystal structure of a synthetic mononuclear nonheme iron(IV)-oxo complex was reported as a chemical model of nonheme iron enzymes in 2003,[1,2] a number of nonheme iron(IV)-oxo complexes have been synthesized and characterized with various spectroscopic methods and X-ray crystallography.[3] Reactivities of the nonheme iron(IV)-oxo complexes have also been investigated intensively in various oxidation reactions, such as C−H bond activation, electron and hydride transfer, and oxygen atom-transfer (OAT) reactions,[4−6] and it has been shown that reactivities of the iron(IV)-oxo complexes are markedly affected by supporting and axial ligands, spin states of the iron(IV) ion, redox-inactive metal ions, and solvents (e.g., pH in aqueous solution).[7−10]

Understanding factors that control reactivities of nonheme iron complexes in oxidation reactions is of importance in designing efficient biomimetic catalysts with high reactivity and selectivity. One important factor that determines reactivities of the iron catalysts is the ligand structure around the iron center.[11] Therefore, iron complexes with various ligand types, such as macrocyclic and tripodal tetradentate N4 ligands and pentadentate N5 ligands, have been synthesized and used as catalysts in oxidation reactions. One notable example is that linear tetradentate N4 ligands can coordinate to an octahedral iron center in three different topologies, *cis*-α, *cis*-*β*, and *trans* forms, as shown in Scheme 1,[12] and the effect of ligand topology has been demonstrated in the catalytic oxidation of olefins and alkanes by nonheme iron(II) complexes and H_2O_2.[13] In particular, the ratio of epoxidation to *cis*-dihydroxylation products in the oxidation of olefins was different depending on the topology of the iron(II) catalysts.[13a,b] Since nonheme iron(IV)-oxo complexes have been considered as active oxidants in the oxidation of organic substrates but the topology effect on their reactivities has never been explored previously, we synthesized nonheme iron(II) complexes with two different topologies, *cis*-α- and *cis*-*β*-[$\mathrm{Fe^{II}(BQCN)(CH_3CN)_2}$]$^{2+}$,[13d,14] and their corresponding iron(IV)-oxo complexes. The *cis*-α and *cis*-*β* isomers of [$\mathrm{Fe^{IV}(O)(BQCN)}$]$^{2+}$ were characterized with various spectroscopic methods, and their structures were proposed by density functional theory (DFT) calculations. More importantly, the effect of the ligand topology on the reactivities of nonheme iron(IV)-oxo complexes has been demonstrated for the first time in C−H bond activation and OAT reactions. The difference in the reactivities of the *cis*-α and *cis*-*β* isomers of [$\mathrm{Fe^{IV}(O)(BQCN)}$]$^{2+}$ was rationalized with the redox potentials of the iron(IV)-oxo complexes.

Scheme 1

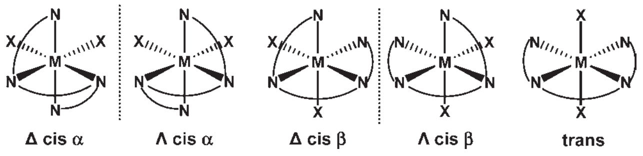

The reaction of BQCN ligand with iron(II) salts, $\mathrm{Fe^{II}(ClO_4)_2}$ and $\mathrm{Fe^{II}(CF_3SO_3)_2}$, afforded iron(II) complexes with different topologies, *cis*-α-[$\mathrm{Fe^{II}(BQCN)(CH_3CN)_2}$]$\mathrm{(ClO_4)_2}$ (**1a**) and *cis*-*β*-[$\mathrm{Fe^{II}(BQCN)(CH_3CN)_2}$]$\mathrm{(CF_3SO_3)_2}$ (**1b**) in CH_3CN, respectively (see Figure 1a,b for the crystal structures of **1a** and **1b**; see Supporting Information (SI) for experimental procedures and for the spectroscopic and structural characterization of **1a** and **1b**).[15] In these structures, the *N*-methyl groups of the BQCN ligand have different configurations in the two topologies: *anti* relative to each other in the *cis*-α isomer and *syn* in the *cis*-*β* isomer. These isomers do not interconvert in solution at 25 °C, as confirmed by ^{1}H NMR spectroscopy and cyclic voltammetry. The ^{1}H NMR spectra of **1a** and **1b** exhibit distinct signals (SI, Figure S2), indicating that there is only one isomer in each solution and that they each retain their respective ligand topologies in solution, even at room temperature. The $\mathrm{Fe^{III/II}}$ redox potential of **1a**, obtained by cyclic voltammetry in CH_3CN at 25 °C, is 1.16 V vs SCE, whereas that of **1b** is 1.09 V vs SCE (SI, Figure S3). The distinct voltammetric behaviors

Received: May 1, 2011
Published: July 07, 2011

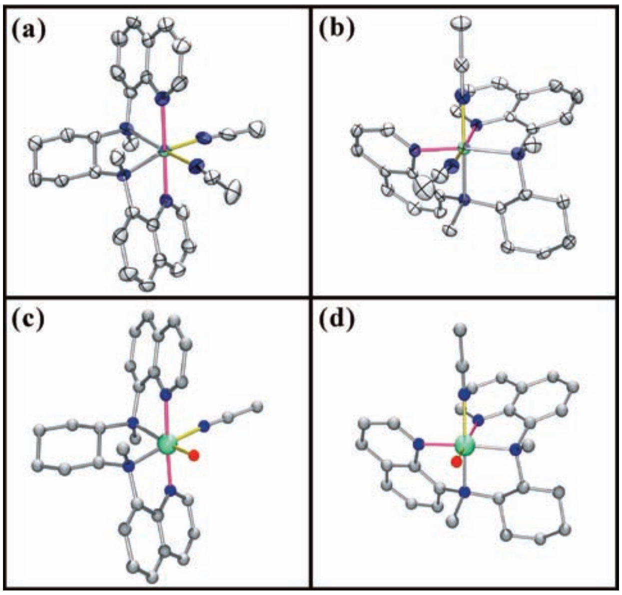

Figure 1. X-ray structures of $[Fe^{II}(BQCN)(CH_3CN)_2]^{2+}$ cations in (a) *cis*-α-$[Fe^{II}(BQCN)(CH_3CN)_2](ClO_4)_2$ (**1a**) and (b) *cis*-*β*-$[Fe^{II}(BQCN)(CH_3CN)_2](CF_3SO_3)_2$ (**1b**), showing 30% probability ellipsoids. DFT-optimized structures of (c) *cis*-α-$[Fe^{IV}(O)(BQCN)]^{2+}$ (**2a**) and (d) *cis*-*β*-$[Fe^{IV}(O)(BQCN)]^{2+}$ (**2b**), calculated at the B3LYP/LANL2DZ level. Hydrogen atoms are omitted for clarity (Fe, green; N, blue; O, red; C, gray). Crystallographic and structural data for **1a** and **1b** are listed in SI, Tables S1 and S2.

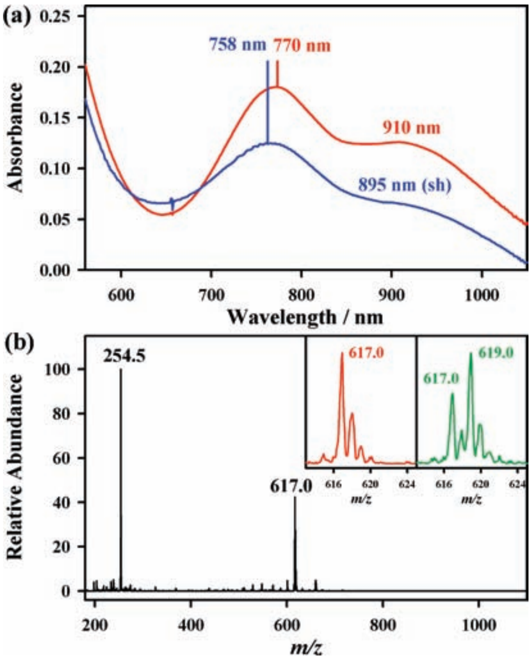

Figure 2. (a) UV–vis spectra of **2a** (blue) and **2b** (red) generated in the reactions of **1a** (1 mM) and **1b** (1 mM) with PAA (3 equiv) in CH_3CN at 0 °C, respectively. (b) ESI-MS of **2b**. The intermediate was generated by reacting **1b** (1 mM) and PAA (3 equiv) in CH_3CN at 0 °C. Insets show the observed isotope distribution patters for **2b**-^{16}O (left panel) and **2b**-^{18}O (right panel). **2b**-^{18}O was generated in the reaction of **1b** (1 mM) and PAA (3 equiv) in the presence of $H_2{}^{18}O$ (10 μL) in CH_3CN at 0 °C, and the ESI-MS was taken after 5 min incubation.

of **1a** and **1b** also support that the topologies of the BQCN ligand in the iron(II) complexes are maintained without being interconverted in solution at room temperature.

Addition of peracetic acid (PAA, 3 equiv) to reaction solutions containing **1a** and **1b** gave a pale green intermediate **2a** with an absorption band at 758 nm ($\varepsilon \approx 120\ M^{-1}\ cm^{-1}$) and a yellowish green intermediate **2b** with an absorption band at 770 nm ($\varepsilon \approx 180\ M^{-1}\ cm^{-1}$), respectively, in CH_3CN at 0 °C (Figure 2a and SI, Figure S4, showing spectral changes for the formation of **2a** and **2b**). The intermediates **2a** and **2b**, which were metastable in CH_3CN at 0 °C ($t_{1/2} \approx 1.5$ h), were characterized by various spectroscopic techniques. The X-band EPR spectra of **2a** and **2b** were silent (data not shown), as reported in nonheme iron(IV)-oxo complexes.[3b] The spin states of **2a** and **2b** were then determined using Evans's NMR method,[16] and the magnetic moments of 3.3 and 3.4 μ_B for **2a** and **2b**, respectively, indicate that the intermediates possess $S = 1$ spin state in CH_3CN solution. The electrospray ionization mass spectrum (ESI-MS) of **2b** exhibited two prominent ion peaks at m/z 254.5 and 617.0 (Figure 2b), whose mass and isotope distribution patterns correspond to $[Fe^{IV}(O)(BQCN)(CH_3CN)]^{2+}$ (calculated m/z 254.6) and $[Fe^{IV}(O)(BQCN)(CF_3SO_3)]^{+}$ (calculated m/z 617.1). Upon introduction of $H_2{}^{18}O$ into the solution of **2b**, a mass shift from m/z 617.0 to 619.0 was observed (Figure 2b, inset), indicating that the oxygen atom of the iron(IV)-oxo species exchanges with labeled water, giving ^{18}O-labeled **2b** with ~70% ^{18}O-incorporation.[17] Similarly, the ESI-MS of **2a** with peak assignment and analysis of oxygen exchange with $H_2{}^{18}O$ is shown in SI, Figure S5. In addition, as illustrated in their starting compounds, **1a** and **1b**, the isomers of iron(IV)-oxo intermediates, **2a** and **2b**, do not interconvert in CH_3CN at 0 °C. The ^1H NMR spectra of **2a** and **2b** exhibit distinct peaks (SI, Figure S6),[18] indicating that there is only one intermediate in solution and that they each retain their respective ligand topologies in solution. The $Fe^{IV/III}$ redox potential of **2a**, obtained by cyclic voltammetry in CH_3CN at 0 °C, was 0.72 V vs SCE, whereas that of **2b** was 0.61 V vs SCE (SI, Figure S7). The distinct voltammetric behaviors of **2a** and **2b** further support that the topologies of the BQCN ligand in the iron(IV)-oxo complexes are maintained without being interconverted in solution. Furthermore, it is worth noting that the redox potentials of both **2a** and **2b** are significantly higher than those of $[Fe^{IV}(O)(N4Py)]^{2+}$ (0.51 V vs SCE), $[Fe^{IV}(O)(Bn\text{-}TPEN)]^{2+}$ (0.49 V vs SCE), and $[Fe^{IV}(O)(TMC)]^{2+}$ (0.39 V vs SCE), but slightly lower than that of $[Fe^{IV}(O)(Bispidine)]^{2+}$ (0.73 V vs SCE).[5a,d,14]

DFT calculations at B3LYP/6-311+G(d,p)//LANL2DZ level[19] using the Gaussian 09 package[20] were performed to elucidate the structural details of **2a** and **2b** (see SI). Due to symmetry, the oxo position in **2a** is always *trans* to an amine nitrogen (Figure 1c), but there are two possibilities for the oxo position in **2b**: *trans* to either a quinolyl nitrogen or an amine nitrogen (Figure 1d and SI, Figure S8). The DFT calculations show that the structure having the oxo atom *trans* to a quinolyl nitrogen is, by 2.4 kcal mol^{-1}, more stable than that having the oxo atom *trans* to an amine nitrogen (see also SI, Table S4). This energy difference is of a scale that is usually reliable at this level of theory when just looking at isomeric differences, as we do here. Therefore, a tentative conclusion based on the calculations is that the observed **2b** has the oxo atom *trans* to a quinolyl nitrogen. The gas-phase calculated Fe═O bond lengths of **2a** and **2b** are 1.66/1.65 Å (SI, Table S5), similar to those found in crystal structures of nonheme iron(IV)-oxo complexes with $S = 1$ spin state, such as $[Fe^{IV}(O)(TMC)]^{2+}$ and $[Fe^{IV}(O)(N4Py)]^{2+}$.[1,18] The singly occupied valence electron orbitals are as usual in

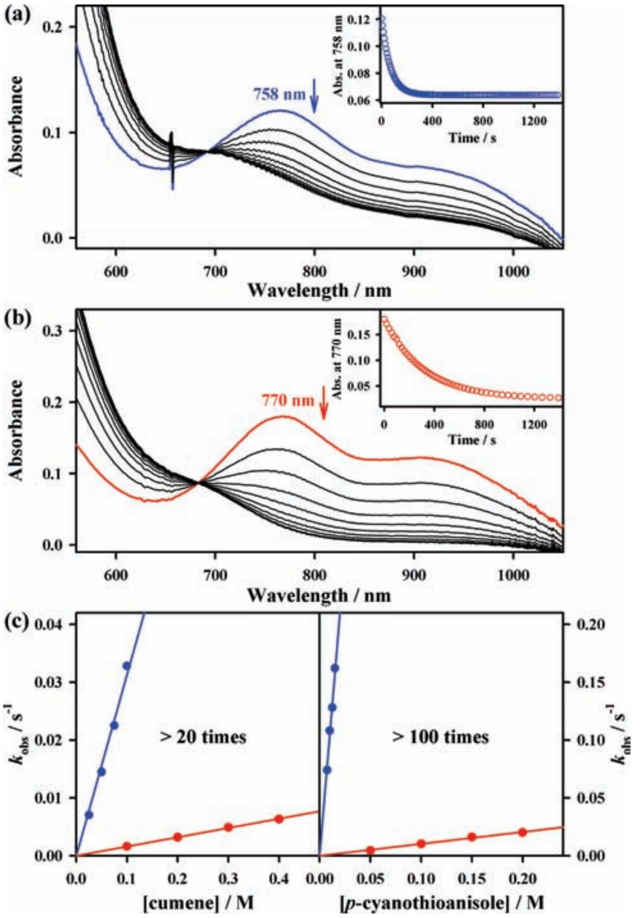

Figure 3. (a) UV–vis spectral changes of **2a** (1 mM, blue) upon addition of cumene (50 mM) in CH_3CN at 0 °C. Inset shows the time course of the decay of **2a** monitored at 758 nm. (b) UV–vis spectral changes of **2b** (1 mM, red) upon addition of cumene (200 mM) in CH_3CN at 0 °C. Inset shows the time course of the decay of **2b** monitored at 770 nm. (c) Plots of k_{obs} vs concentrations of cumene at 0 °C (left) and *p*-cyanothioanisole at −40 °C (right) to determine second-order rate constants for the reactions of **2a** (blue) and **2b** (red).

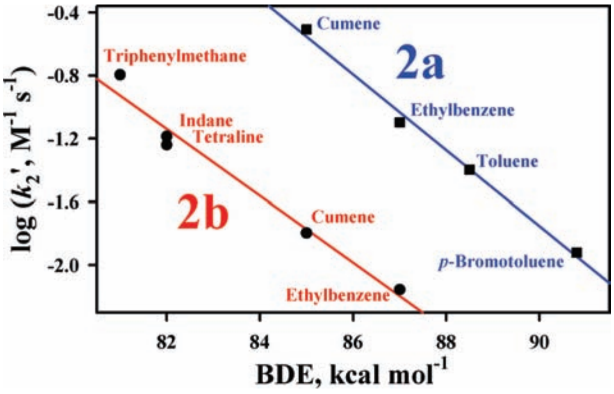

Figure 4. Plot of log k'_2 of **2a** (■, blue) and **2b** (●, red) against C−H BDE of substrates. Second-order rate constants, k_2, were determined in CH_3CN at 0 °C and then adjusted for the reaction stoichiometry to yield k'_2 based on the number of equivalent target C−H bonds of substrates: one for triphenylmethane and cumene, two for ethylbenzene, three for toluene and *p*-bromotoluene, and four for indane and tetraline.

nonheme $Fe^{IV}O$ cases, such as two perpendicular π^* orbitals with about one spin on Fe and O each (SI, Table S6).

The reactivities of **2a** and **2b** were investigated with substrates having C−H bond dissociation energies (BDEs) in the range of 81−91 kcal mol^{-1}, such as triphenylmethane, indane, tetraline, cumene, ethylbenzene, toluene, and *p*-bromotoluene.[21] Upon addition of cumene (50 mM) to a solution of **2a**, the intermediate reverted back to the starting **1a** (Figure 3a), yielding 2-phenyl-2-propanol quantitatively. When the cumene oxidation was performed with ^{18}O-labeled **2a** (i.e., **2a**-^{18}O), the oxygen in the 2-phenyl-2-propanol product derived from the ^{18}O-labeled iron-oxo species (SI, experimental details). The latter result demonstrates that **2a** was the oxidant giving the oxidized product and that the oxygen in the product did not come from O_2. First-order rate constants, determined by the pseudo-first-order fitting of the kinetic data for the decay of **2a**, increased linearly with the increase of the cumene concentration (Figure 3c, left panel, blue circles), yielding a second-order rate constant (k_2) of 3.1(2) × 10^{-1} M^{-1} s^{-1}. Similarly, the k_2 value of **2b** was determined to be 1.6(2) × 10^{-2} M^{-1} s^{-1} in the oxidation of cumene (Figure 3c, left panel, red circles). These results indicate that **2a** is ~20 times more reactive than **2b** in this reaction. Similarly, second-order rate constants of **2a** and **2b** were determined in the oxidation of other substrates, showing that **2a** is more reactive than **2b** in these C−H bond activation reactions (Figure 4; also see SI, Table S3). Furthermore, kinetic isotope effect (KIE) values of 7 and 9 were obtained in the oxidation of ethylbenzene by **2a** and **2b**, respectively (SI, Figure S9 and Table S3). As suggested previously, the observations of the good correlation between reaction rates and BDEs of substrates and large KIE values propose that the C−H bond activation by **2a** and **2b** occurs via an H-atom abstraction mechanism.[3b,4a,4f,7]

OAT reactions were also investigated in the oxidation of thioanisole derivatives by **2a** and **2b** in CH_3CN at −40 °C. Upon addition of *p*-cyanothioanisole to the solutions of **2a** and **2b**, the intermediates reverted back to **1a** and **1b**, respectively, yielding *p*-cyanophenyl methyl sulfoxide quantitatively. The rate constants of **2a** and **2b** increased linearly with increasing *p*-cyanothioanisole concentration (Figure 3c, right panel; SI, Table S3), leading us to determine k_2 = 1.0(2) × 10 and 1.0(2) × 10^{-1} M^{-1} s^{-1} for the reactions of **2a** and **2b**, respectively. Similarly, reaction rates were determined in the oxidation of *p*-nitrothioanisole by **2a** and **2b**, giving k_2 = 6.0(3) and 5.3(2) × 10^{-2} M^{-1} s^{-1}, respectively (SI, Table S3). These results demonstrate that the reactivity of **2a** is greater than that of **2b** by 2 orders of magnitude in OAT reactions.

Why, then, is **2a** more reactive than **2b** in the C−H bond activation and OAT reactions? We have shown above that the $Fe^{IV/III}$ redox potential of **2a** (0.72 V vs SCE) is higher than that of **2b** (0.61 V vs SCE) by 0.11 V, indicating that **2a** is a stronger oxidant than **2b**. In general, the oxidant with a more positive potential exhibits a greater reactivity in oxidation reactions.[5a] Indeed, when we determined activation parameters (e.g., $\Delta G^{\ddagger}$) in the oxidation of cumene by **2a** and **2b**, the $\Delta G^{\ddagger}$ value of **2a** (18.6 kcal mol^{-1}) was 1.6(2) kcal mol^{-1} lower than that of **2b** (20.2 kcal mol^{-1}) at 0 °C (SI, Figure S10). We therefore conclude that *cis*-α-$[Fe^{IV}(O)(BQCN)]^{2+}$ (**2a**) with a high $Fe^{IV/III}$ redox potential is more reactive than *cis*-*β*-$[Fe^{IV}(O)(BQCN)]^{2+}$ (**2b**) with a low $Fe^{IV/III}$ redox potential in the activation of C−H bonds and the oxidation of sulfides.

In summary, we have shown that the linear tetradentate BQCN ligand coordinates to an octahedral Fe^{II} center in two different topologies (i.e., *cis*-α and *cis*-*β*), depending on the anions of iron salts (i.e., $Fe^{II}(ClO_4)_2$ and $Fe^{II}(CF_3SO_3)_2$). We have also shown that iron(IV)-oxo complexes with two different topologies, *cis*-α-$[Fe^{IV}(O)(BQCN)]^{2+}$ and *cis*-*β*-$[Fe^{IV}(O)(BQCN)]^{2+}$, are generated from their corresponding iron(II) complexes. The topologies of the BQCN ligand in these iron(IV)-oxo complexes as well as in the iron(II) complexes are maintained without being interconverted in solution at room temperature. The *cis*-α-$[Fe^{IV}(O)(BQCN)]^{2+}$ complex is more reactive than the *cis*-*β*-$[Fe^{IV}(O)(BQCN)]^{2+}$ complex in C−H bond activation and sulfide oxidation reactions. The reactivity difference of the *cis*-α and *cis*-*β* isomers of $[Fe^{IV}(O)(BQCN)]^{2+}$ is rationalized with their $Fe^{IV/III}$ redox potentials: the redox potential of *cis*-α isomer is 0.11 V higher than that of *cis*-*β* isomer. The present results demonstrate that the ligand topology is an important factor that contributes to the oxidizing power of nonheme iron(IV)-oxo complexes in C−H bond activation and oxygen atom-transfer reactions.

■ ASSOCIATED CONTENT

Ⓢ Supporting Information. Experimental details; crystallographic, spectroscopic, and kinetic data; DFT section; and complete ref 20. This material is available free of charge via the Internet at http://pubs.acs.org.

■ AUTHOR INFORMATION

Corresponding Author

wwnam@ewha.ac.kr; shinws@sogang.ac.kr

Author Contributions

§These authors contributed equally to this work.

■ ACKNOWLEDGMENT

This work was supported by NRF of Korea through GRL (2010-00353) and WCU (R31-2008-000-10010-0) (W.N.), 2011 KRICT OASIS project (W.N.), and NRF (2009-C1AAA001-2009-0093879) (W.S.).

■ REFERENCES

(1) Rohde, J.-U.; In, J.-H.; Lim, M. H.; Brennessel, W. W.; Bukowski, M. R.; Stubna, A.; Münck, E.; Nam, W.; Que, L., Jr. *Science* **2003**, *299*, 1037.

(2) (a) Abu-Omar, M. M.; Loaiza, A.; Hontzeas, N. *Chem. Rev.* **2005**, *105*, 2227. (b) Krebs, C.; Fujimori, D. G.; Walsh, C. T.; Bollinger, J. M., Jr. *Acc. Chem. Res.* **2007**, *40*, 484.

(3) (a) Nam, W. *Acc. Chem. Res.* **2007**, *40*, 465 and review articles in the special issue. (b) Nam, W. *Acc. Chem. Res.* **2007**, *40*, 522. (c) Bruijnincx, P. C. A.; van Koten, G.; Klein Gebbink, R. J. M. *Chem. Soc. Rev.* **2008**, *37*, 2716. (d) Borovik, A. S. *Chem. Soc. Rev.* **2011**, *40*, 1870.

(4) (a) Kaizer, J.; Klinker, E. J.; Oh, N. Y.; Rohde, J.-U.; Song, W. J.; Stubna, A.; Kim, J.; Münck, E.; Nam, W.; Que, L., Jr. *J. Am. Chem. Soc.* **2004**, *126*, 472. (b) Balland, V.; Charlot, M.-F.; Banse, F.; Girerd, J.-J.; Mattioli, T. A.; Bill, E.; Bartoli, J.-F.; Battioni, P.; Mansuy, D. *Eur. J. Inorg. Chem.* **2004**, 301. (c) Oh, N. Y.; Suh, Y.; Park, M. J.; Seo, M. S.; Kim, J.; Nam, W. *Angew. Chem., Int. Ed.* **2005**, *44*, 4235. (d) Martinho, M.; Banse, F.; Bartoli, J.-F.; Mattioli, T. A.; Battioni, P.; Horner, O.; Bourcier, S.; Girerd, J.-J. *Inorg. Chem.* **2005**, *44*, 9592. (e) Comba, P.; Maurer, M.; Vadivelu, P. *J. Phys. Chem. A* **2008**, *112*, 13028. (f) Seo, M. S.; Kim, N. H.; Cho, K.-B.; So, J. E.; Park, S. K.; Clémancey, M.; Garcia-Serres, R.; Latour, J.-M.; Shaik, S.; Nam, W. *Chem. Sci.* **2011**, *2*, 1039.

(5) (a) Lee, Y.-M.; Kotani, H.; Suenobu, T.; Nam, W.; Fukuzumi, S. *J. Am. Chem. Soc.* **2008**, *130*, 434. (b) Fukuzumi, S.; Kotani, H.; Lee, Y.-M; Nam, W. *J. Am. Chem. Soc.* **2008**, *130*, 15134. (c) Fukuzumi, S.; Kotani, H.; Suenobu, T.; Hong, S.; Lee, Y.-M.; Nam, W. *Chem.—Eur. J.* **2010**, *16*, 354. (d) Comba, P.; Fukuzumi, S.; Kotani, H.; Wunderlich, S. *Angew. Chem., Int. Ed.* **2010**, *49*, 2622.

(6) (a) Park, M. J.; Lee, J.; Suh, Y.; Kim, J.; Nam, W. *J. Am. Chem. Soc.* **2006**, *128*, 2630. (b) Sastri, C. V.; Oh, K.; Lee, Y. J.; Seo, M. S.; Shin, W.; Nam, W. *Angew. Chem., Int. Ed.* **2006**, *45*, 3992.

(7) Sastri, C. V.; Lee, J.; Oh, K.; Lee, Y. J.; Lee, J.; Jackson, T. A.; Ray, K.; Hirao, H.; Shin, W.; Halfen, J. A.; Kim, J.; Que, L., Jr.; Shaik, S.; Nam, W. *Proc. Natl. Acad. Sci. U.S.A.* **2007**, *104*, 19181.

(8) (a) Pestovsky, O.; Stoian, S.; Bominaar, E. L.; Shan, X.; Münck, E.; Que, L., Jr.; Bakac, A. *Angew. Chem., Int. Ed.* **2005**, *44*, 6871. (b) England, J.; Martinho, M.; Farquhar, E. R.; Frisch, J. R.; Bominaar, E. L.; Münck, E.; Que, L., Jr. *Angew. Chem., Int. Ed.* **2009**, *48*, 3622. (c) England, J.; Guo, Y.; Farquhar, E. R.; Young, V. G., Jr.; Münck, E.; Que, L., Jr. *J. Am. Chem. Soc.* **2010**, *132*, 8635. (d) Cho, K.-B.; Shaik, S.; Nam, W. *Chem. Commun.* **2010**, *46*, 4511. (e) Lacy, D. C.; Gupta, R.; Stone, K. L.; Greaves, J.; Ziller, J. W.; Hendrich, M. P.; Borovik, A. S. *J. Am. Chem. Soc.* **2010**, *132*, 12188.

(9) (a) Fukuzumi, S.; Morimoto, Y.; Kotani, H.; Naumov, P.; Lee, Y.-M.; Nam, W. *Nat. Chem.* **2010**, *2*, 756. (b) Morimoto, Y.; Kotani, H.; Park, J.; Lee, Y.-M.; Nam, W.; Fukuzumi, S. *J. Am. Chem. Soc.* **2011**, *133*, 403. (c) Park, J.; Morimoto, Y.; Lee, Y.-M.; Nam, W.; Fukuzumi, S. *J. Am. Chem. Soc.* **2011**, *133*, 5236.

(10) (a) Sastri, C. V.; Seo, M. S.; Park, M. J.; Kim, K. M.; Nam, W. *Chem. Commun.* **2005**, 1405. (b) Bautz, J.; Bukowski, M. R.; Kerscher, M.; Stubna, A.; Comba, P.; Lienke, A.; Münck, E.; Que, L., Jr. *Angew. Chem., Int. Ed.* **2006**, *45*, 5681.

(11) (a) Que, L., Jr.; Tolman, W. B. *Nature* **2008**, *455*, 333. (b) Bigi, M. A.; Reed, S. A.; White, M. C. *Nat. Chem.* **2011**, *3*, 216.

(12) (a) Aldrich-Wright, J. R.; Vagg, R. S.; Willams, P. A. *Coord. Chem. Rev.* **1997**, *166*, 361. (b) Gavrilova, A. L.; Bosnich, B. *Chem. Rev.* **2004**, *104*, 349.

(13) (a) Costas, M.; Que, L., Jr. *Angew. Chem., Int. Ed.* **2002**, *41*, 2179. (b) Mas-Ballesté, R.; Costas, M.; van den Berg, T.; Que, L., Jr. *Chem.—Eur. J.* **2006**, *12*, 7489. (c) Britovsek, G. J. P.; England, J.; White, A. J. P. *Dalton Trans.* **2006**, 1399. (d) England, J.; Britovsek, G. J. P.; Rabadia, N.; White, A. J. P. *Inorg. Chem.* **2007**, *46*, 3752.

(14) Abbreviations used: BQCN, *N*,*N*′-dimethyl-*N*,*N*′-bis(8-quinolyl)-cyclohexanediamine; N4Py, *N*,*N*-bis(2-pyridylmethyl)-*N*-bis(2-pyridyl)-methylamine; Bn-TPEN, *N*-benzyl-*N*,*N*′,*N*′-tris(2-pyridylmethyl)ethane-1,2-diamine; TMC, 1,4,8,11-tetramethyl-1,4,8,11-tetraazacyclotetradecane.

(15) Two different crystal structures with the same topology (i.e., *cis*-*β* form) were obtained in the Fe^{II}(BQCN) complex prepared using $Fe^{II}(CF_3SO_3)_2$, one coordinating two acetonitrile molecules (**1b**) and the other coordinating two triflate anions (**1b**′; SI, Figure S1). These complexes, **1b** and **1b**′, are in equilibrium in CH_3CN solution. See ^1H NMR spectra of **1a** and **1b** in SI, Figure S2, for further discussion.

(16) (a) Evans, D. F. *J. Chem. Soc.* **1959**, 2003. (b) Evans, D. F.; Jakubovic, D. A. *J. Chem. Soc., Dalton Trans.* **1988**, 2927.

(17) (a) Seo, M. S.; In, J.-H.; Kim, S. O.; Oh, N. Y.; Hong, J.; Kim, J.; Que, L., Jr.; Nam, W. *Angew. Chem., Int. Ed.* **2004**, *43*, 2417. (b) Yoon, J.; Wilson, S. A.; Jang, Y. K.; Seo, M. S.; Nehru, K.; Hedman, B.; Hodgson, K. O.; Bill, E.; Solomon, E. I.; Nam, W. *Angew. Chem., Int. Ed.* **2009**, *48*, 1257.

(18) A ^1H NMR spectrum of a nonheme iron(IV)-oxo complex, $[Fe^{IV}(O)(N4Py)]^{2+}$, was reported: Klinker, E. J.; Kaizer, J.; Brennessel, W. W.; Woodrum, N. L.; Cramer, C. J.; Que, L., Jr. *Angew. Chem., Int. Ed.* **2005**, *44*, 3690.

(19) (a) Becke, A. D. *Phys. Rev. A* **1988**, *38*, 3098. (b) Becke, A. D. *J. Chem. Phys.* **1993**, *98*, 1372. (c) Becke, A. D. *J. Chem. Phys.* **1993**, *98*, 5648. (d) Lee, C.; Yang, W.; Parr, R. G. *Phys. Rev. B* **1988**, *37*, 785. (e) Perdew, J. P. *Phys. Rev. B* **1986**, *33*, 8822.

(20) Frisch, M. J.; et al. . *Gaussian 09*; Gaussian, Inc.: Wallingford, CT, 2010.

(21) Luo, Y.-R. *Handbook of bond dissociation energies in organic compounds*; CRC Press: New York, 2003.